Analytica Chimica Acta 1225 (2022) 340224

Contents lists available at ScienceDirect

Analytica Chimica Acta

journal homepage: www.elsevier.com/locate/aca

A systematic evaluation on the impact of sample-related and environmental factors in the analytical performance of acoustic emission from laser-induced plasmas

Markéta Bosáková [a,b,1], Pablo Purohit [a,c,1], César Alvarez-Llamas [a], Javier Moros [a,**], Karel Novotný [b], Javier Laserna [a,*]

[a] UMALaserlab, Departamento de Química Analítica, Universidad de Málaga, Jiménez Fraud 4th, 29010, Málaga, Spain
[b] Department of Chemistry, Masaryk University, Kamenice 5, Brno, 625 00, Czech Republic
[c] Niels Bohr Institute, University of Copenhagen, Blegdamsvej 17, 2100, Copenhagen, Denmark

HIGHLIGHTS

- Laser-induced plasmas acoustics is a potential source of analytical information.
- Inner and outer variables to the inspected target may alter the generated acoustics.
- Systematic tests were conducted to define implications on the recorded acoustics.
- Peculiarities of plasmaphonies may reveal related attributes of solids.

GRAPHICAL ABSTRACT

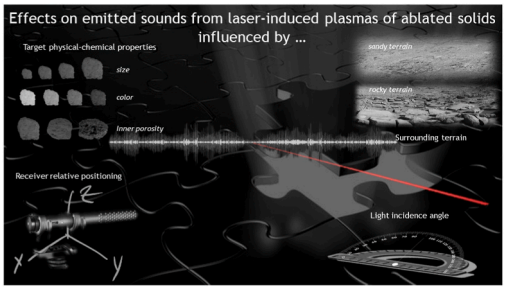

ARTICLE INFO

Keywords:
Acoustics
Plasmas
Laser
Plasmaphony
Solids

ABSTRACT

Acoustics recordings from laser-induced plasmas are becoming increasingly regarded as a complementary source of information from the inspected sample. The propagation of these waves is susceptible to be modified by the physicochemical traits of the sample, thus yielding specific details that can be used for sorting and identification of targets. Still, the relative fragility of the acoustic wave poses major challenges to the applicability of laser-induced acoustics. Echoes and reflections sourcing from intrasample parameters as well as from interactions of the acoustic wave with the surroundings of the inspected target can dilute the analytical information directly related to the object contained within the recordings. The present work aims to experimentally scrutinize the impact of different parameters internal and external to the sample into the final acoustic signal from laser-induced plasmas in order to accurately use this information source for characterization purposes. Variables inherent to the sample such as dimensions, porosity and absorption coefficient, which guides the laser-matter coupling process, have been, for the first time, systematically studied using ad-hoc solids to thoroughly isolate their influence on the signal. Moreover, modulation of soundwave induced by the surroundings of the probed

* Corresponding author.
** Corresponding author.
E-mail addresses: j.moros@uma.es (J. Moros), laserna@uma.es (J. Laserna).
[1] These authors contributed equally and are joint first authors.

https://doi.org/10.1016/j.aca.2022.340224
Received 10 May 2022; Received in revised form 15 July 2022; Accepted 31 July 2022
Available online 3 August 2022

target and the anisotropy of the acoustic signal because of the angle at which the plasma is formed, have been evaluated.

1. Introduction

Upon irradiation with a focused laser pulse, and provided a certain threshold energy density value is reached, probed materials undergo several macroscopic processes such as ablation and plasma formation. The first phenomena consist in the transference of a fraction of mass from the sample, commonly a solid, into the vapor phase [1–3]. Laser ablation (LA) has become a popular straightforward pathway for the fabrication of thin layers, structured surfaces and nanoparticles as controlled irradiation and subsequent condensation settings allow access to a wide variety of morphologies [4–7]. In the second case, the produced plasmas contain atoms freed from the inspected sample in light-emissive states. Yielded photons can, therefore, be recorded in order to obtain analytical information concerning the elemental composition of the sample. This technique is known as laser-induced breakdown spectroscopy (LIBS) [8–10]. Ablation and plasma formation, under both below and above formation threshold conditions, are accompanied by the generation of shockwaves. Owing to the deformations caused by the laser pulse, shockwaves propagate along the surface and within the irradiated objects causing them to vibrate and, as the material is expelled from its original matrix, emit recordable sound waves [11,12]. Laser-induced plasma acoustics (LIPAc) has been proposed as a mean to expand the information regarding the target via the intensity of the recorded signal. In the context of LA, acoustics can be useful as an internal standard in order to correct shot-to-shot fluctuations and, after calibration, infer the amount of material ablated in each laser shot [13,14]. For LIBS, acoustics have been tested to reveal additional traits related to the physical and compositional characteristics of the target [15,16]. Despite the interest shown in LIPAc for the aforementioned purposes, the multiple sources of uncertainty linked to sound waves have hindered their potential application in in-lab as well as off-lab sensors. Acoustic signal pollution arises mainly from the interaction of the resulting sound field, which will be referred to henceforth as plasmaphony, with the sample's surrounding as it propagates in all directions before reaching the receiver where it is detected. Therefore, numerous echoes, reflections and interferences are bound to be captured alongside the signal truly belonging to the sample, thus diluting it and burdening the interpretation of data.

Recently, literature has highlighted the potential of plasmaphonics to address physical traits of the samples such as hardness [17] or, even, chemical features such as the content in NaCl owing to changes in the speed of sound in the samples or laser-induced phase changes [10]. It is also worth noting that the Perseverance rover deployed as part of the latest Mars-surveying NASA mission, Mars 2020 also features a microphone that can be operated in synchronization with the LIBS laser, allowing the evaluation of the correlation and the complementation between spectroscopic and acoustic measurements [18]. The aforementioned events have re-kindled the motivation towards comprehending the different phenomena taking place during the lifetime of the shockwave in order to extract from it the contribution of the inspected sample [19–23]. These sounds should be able to provide an extended ''picture'' of attributes of the object inaccessible to LIBS in a straightforward way; with the crystal phase in which atoms are arranged being among the most interesting and ambitious prospective traits to be extracted. Yet, to ensure reproducibility, it is crucial to consider the impact of the different variability sources in the rather fragile acoustic signal to ensure that the data under consideration belong only to the chemical nature of the sample. Thus, the fundamental question to be addressed in seeking to further develop this field is: how can the information bore by the plasmaphony be exploited from an analytical point of view? And, also, what information from the object is truly present within the sound wave?

In this work, sets of morphologically-controlled samples coming from chemically identical materials are probed under similar experimental conditions to systematically test the impact of sample-related traits as well as environmentally-induced factors upon the collected audio signal. Geometrical factors such as diameter and length as well as sampling position are explored using aluminum (Al) samples. Sample absorption of the impinging laser light was also tested in Al and plastic samples containing pigments with varying extinction coefficients as this factor conditions the laser-sample coupling and, subsequently, the traits of the resulting plasma. Moreover, *3D*-printed probes of varying wire lengths were used to evaluate how material porosity modified the plasmaphony. Concerning the influence of non-sample derived sources, diverse environmental effects were considered. Changes in the flooring along the sample-to-microphone acoustic propagation path revealed variations in the acoustic spectra after the first peak-to-peak amplitude scoring, a widely used descriptor in laser-induced acoustic studies, thereby indicating the formation of surroundings-dependent interference patterns. Lastly, we tested the microphone-to-sample distance and the height of the microphone with respect to the ground seeking to understand whether small changes in the acoustic path could result in an array of interferences permeating the receptor. Based on these results, the authors quantify how the experimental conditions under which laser-induced acoustics studies are performed alter the collected data and how non-chemical environmental and sample contributions can be avoided in order to yield the robust results required in material analysis.

2. Materials and methods

2.1. Experimental set-up

A schematic of the experimental set-up used in this work is shown in Fig. 1. A pulsed Q-switched Nd:YAG laser (10 Hz, 400 mJ pulse^{-1}, @ 1064 nm, 5.5 ns pulse width) was used as excitation source. Laser pulses of 40 $\pm$ 0.6 mJ in energy were tightly focused on samples by a plane-convex quartz lens of a focal length of 750 mm, thus leading to a spot diameter of ~1 mm at the surface of targets located at a distance of 1 m. Samples were placed on a linear motorized stage to refresh the intra-target sampling position. The sample holder was coated with neoprene to isolate any frequency generated from the vibration of the mechanical equipment. Furthermore, the sample holder was housed inside a custom-built anechoic chamber (145 $\times$ 70 $\times$ 50 cm, L $\times$ W $\times$ H). HiLo-N40 acoustic foam made from polyurethane with high rigidity and low density (70 mm total length, 40 mm knob height, 16.5 $\pm$ 1.0 kg m^{-3} bulk density) was used as the inside absorbent to reduce echoes and resonances as well as vibrations and noise contributions from outside.

The emerging sounds from plasma events were recorded using a 6 mm pre-polarized condenser microphone (20 Hz–19 kHz frequency response, omni-directional polar pattern, 14 mV Pa^{-1} sensitivity, TR-40 model from Audix) also housed inside the anechoic chamber at a fixed sample surface-to-microphone distance of 50 cm and quasi-coaxially to the direction of plasma expansion – an angle of about 10° was used to avoid blocking the optical path of the excitation laser. It is worth noting that the waves shown in the figures across the text were set on a relative time scale to avoid interferences from prior laser-produced shockwaves upon successive pulses. Under accurate synchronization, for a sample surface-to-microphone distance of 50 cm, delay is about 1.5 ms at a speed of sound of 340 m/s. A 24-bit/192 kHz audio interface (UA-55 Quad-capture model from Roland) was used at sampling rate of 96 kHz for digitalization of acoustic waves. Audacity software (version 3.1.3) was employed as audio recording application. During operations, the lab

temperature was real-time monitored at 25 ± 2 °C.

2.2. Samples & scenarios

To investigate the potential dependency of laser-induced acoustic emission on specimen size we decided to analyze a batch of cylindrical solid Al targets with varying diameter and length. Specimen diameters ranged from 10 mm to 50 mm in 10 mm steps. Moreover, for each diameter value, specimens of 1 mm, 5 mm, 10 mm and 20 mm in length were probed. In total, 20 cylinders were fabricated from the same compact plain 2030 Al rod. Details on the characteristics of the alloy are reported in Table S1 in the Supplementary Material.

To evaluate the influence of the material on the recorded signal, epoxy resin cylindrical solids of identical dimensions (30 mm in diameter and 10 mm in length) were prepared. In this case, different calcium-based tempera paints were used to color the epoxy resin cylinders in order to study the impact of the linear absorption coefficient (ε) on the recorded results. The amount of pigment added to the resin was restricted to the minimum to ensure full coloration seeking to avoid matrix effects altering the acoustic signal. A total of 6 colored cylinders (red, green, blue, yellow, black, and white) and a non-colored cylinder, acting as reference, were prepared from the same epoxy mixture. In addition, similar cylinders of 30 mm in diameter and 10 mm in length were modeled and *3D*-printed with varying porosity. Printable plastic filaments of two different lengths (detailed in the corresponding subsection) were used and 3 specimens from each filament were printed. Thus, a total of 6 cylinders featuring particular, homogenous and uniformly-distributed inner porosity (as characterized by volumetric measurement), size, and pore shape, were evaluated.

The surface over which plasmaphony propagates may significantly affect its temporal profile. To investigate how the surrounding terrain can adulterate the plasmaphony, different scenarios were considered. First, a ground featuring sound absorptive material was used. The polyurethane acoustic foam partially counteracts the effects of sound reflection by the optical table and, thus, helps to reduce the noise level. Also, more realistic terrains like stony ground and sandy ground were designed. All scenarios were conveniently adapted to cover the 50 cm × 50 cm area between the emitter source and the receiver device, i.e., the microphone.

3. Results and discussion

3.1. Effect of the size of solids on acoustic waves

First, the influence of the sample morphology and the sampling spot on the recorded acoustic signal was evaluated. The main goal was to confirm whether materials of identical composition yield responses conditioned by their dimensions (i.e., diameter and length) and the physical surroundings of the sampled surface coordinate as the quantity of material neighboring the irradiated zone may alter the transmission of the sound wave and lead to the formation of delayed interferences and echoes perturbing the sample-related signal.

Fig. 2A shows representative sound waves from solid Al cylinders of 30 mm in diameter and increasing lengths in the time domain. Data correspond to the average of 20 laser-induced plasmaphonies at the geometrical center of the specimens' surface. Upon inspection of the recorded acoustic responses, three main sections can be identified during the signal lifetime. The first segment ranged from the first detectable microphone membrane vibration up to the first minimum of the acoustic signal. This segment encompassed the largest max-to-min amplitude value, located from ~ 0.5 ms to 0.6 ms. It is worth noting that, all specimens, no matter their length, featured nearly identical acoustic amplitude values (calculated from the absolute value of the intensity maximum and minimum, $A = I_{max} - I_{min}$) as shown in Fig. 2A. This observation is consistent with the produced wave being intimately associated to the particular characteristics of the interaction between the laser and the sample. Therefore, common influential parameters of the laser-matter interaction guided the magnitude of the amplitude, with those variables being the laser pulse properties (duration (τ), wavelength (λ) and fluence ($F = J{\cdot}cm^{-2}$)) and the physical traits of the material (ε, hardness, …) [24]. The second segment covered from 0.6 ms to 1.2 ms; a lapse within which dimensions-mediated differences were present. In order to explain these differences, the cylinder surface (a circle) can be considered as a membrane attached at its ends, thus delimiting its bearing edges. When vibrating, each membrane, depending on its dimensions, produces different modes whose nodes are diametrical lines, circular lines and a combination of both. Moreover, each vibration mode produces a series of frequencies which are not integer multiples of the fundamental frequency (hence they are called "overtones", "partials" or "concomitants" instead of harmonics), responsible for "coloring" the sound and producing timbral differences, that is, variations within the relative amplitudes of the spectral components [25,26]. To verify the idea of overtones inducing the recorded differences, Fig. 3 compares representative sound waves from Al

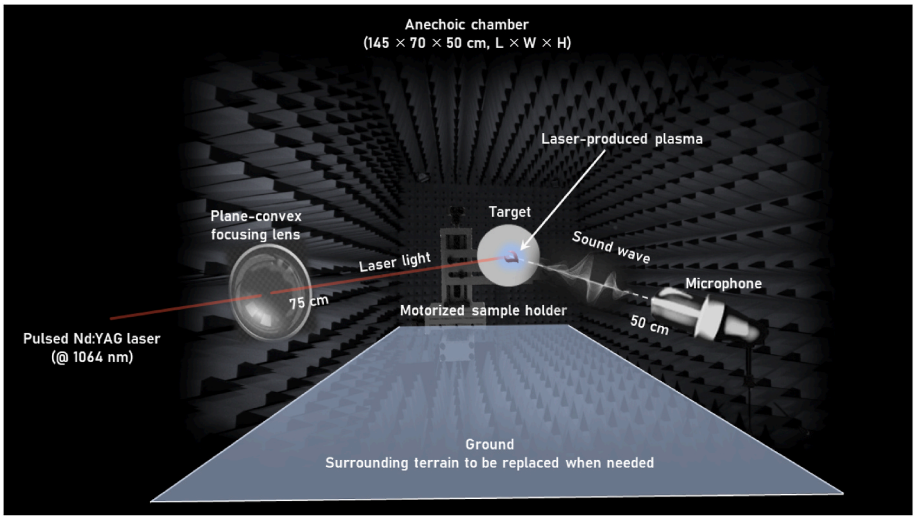

Fig. 1. Experimental set-up scheme.

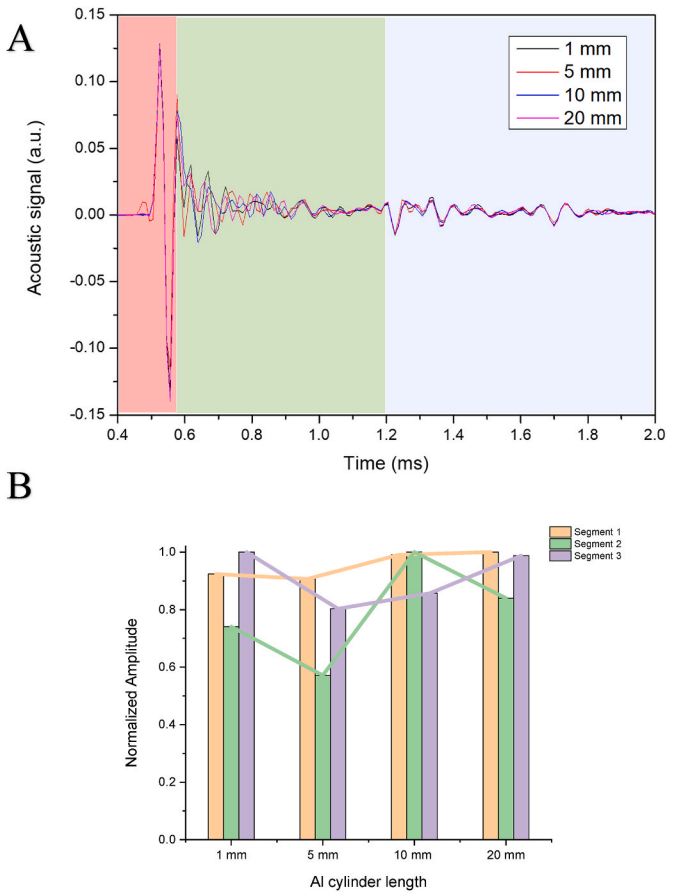

Fig. 2. A) Representative sound waves featuring segments discussed in the main text for a fixed sample diameter of 30 mm. In red is segment 1, segment 2 is green and segment 3 is blue. B) Normalized amplitude for the acoustic signal within each segment identified in A), from Al cylindrical solids of 30 mm in diameter but different in length. Data correspond to the average of 60 laser-induced plasmaphonies at the center of the specimens' surface. (For interpretation of the references to color in this figure legend, the reader is referred to the Web version of this article.)

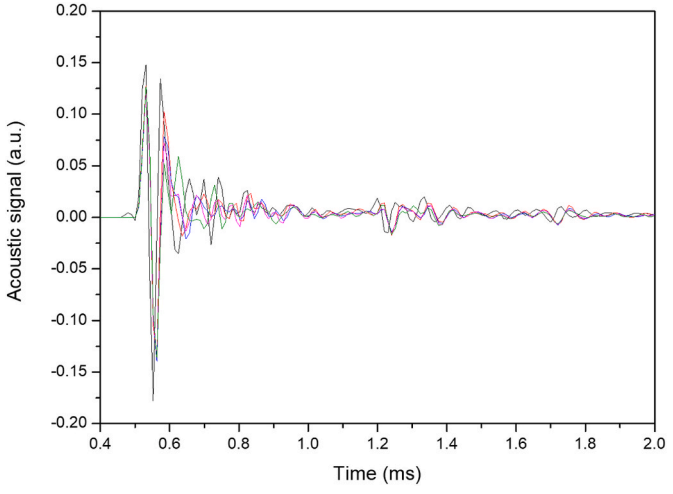

Fig. 3. Average signal from 60 events recorded on 3 central positions over the surface of Al targets of 10 mm in length and increasing diameters ranging from 10 mm to 50 mm in 10 mm steps.

cylinders of variable diameter, ranging from 10 mm to 50 mm in 10 mm steps, while keeping their length constant at 10 mm. In the displayed data, 60 events taken at three central spots over the surface of the samples were averaged. This is a common practice in LIBS experiments in order to avoid drilling effects. When the laser pulse hit the central part of the surface of each cylinder, due to their different diameters, the vibration mode (0,1) which has a circular node and no diametral node, and is responsible for the fundamental frequency, is expected to vary slightly; hence the exiguous dissimilarities in the second segment of their acoustic waves [27]. Fig. 4A displays the max-to-min amplitude for the first maximum. On the other hand, data in Fig. 4B show the max-to-min amplitude for the absolute maximum present in the aforementioned second segment. Upon comparison of both datasets, the larger disparities in Fig. 4B (easily identifiable from the different scales for the y-axis in the A and B charts) agreed with a change in the main influence modulating the acoustic signal, i.e., a shift from laser-matter interaction to sample vibration. This shift was significantly more pronounced for cylinders of the smallest length (1 mm), no matter their diameters, which are prone to magnify the vibrations transmitted through them. The same argument applies to the acoustic mode when the laser pulse hit the same cylinder at the edge of the surface, i.e., in a peripheral spot. These results were consistently observed for cylinders of identical diameter (for which the surface tension can be assumed identical) but different lengths (the "bearing edge"). The different lengths of the cylinders also modified the fundamental frequency and, consequently, a part of the acoustic signal. Thus, the mismatch identified in the sound waves in the window from 0.6 ms to 1.2 ms can be argued on the basis of the distinct dynamic behavior of a fully clamped circular surface. Lastly, the third segment ranged from 1.2 ms up to signal extinction at ~2.0 ms. Upon comparing the third segments for each sample diameter and length, virtually no differences were found in any case. Also, larger similarities than those observed in the second segment were featured, indicating reduced influence of the vibrational overtones. In consequence, interaction of the original sound wave with its surroundings arises as the main source of the recorded signal at this interval. At longer acquisition times, reflections along the sound path caused by the hemispheric profile of the expanding shockwave as well as roundtrip echoes become predominant, diluting the amount of information directly proceeding from the sample as the sound interacted with neighboring elements. Fig. 2B graphically reflects these arguments. The normalized amplitude for the acoustic signal within each segment was monitored for the Al cylinders of 30 mm in diameter but different length. As can be seen, minute differences are identified in the first segment of the signal, whereas the largest mismatching can be observed within the second segment.

Thus, results from this section highlight the first segment of the recorded laser-induced acoustic wave as the one containing the most direct information concerning the sample. Moreover, as the acquired data is mediated by laser-matter interaction which, under identical operational conditions, is unique to each material, the first amplitude value is confirmed as a reliable tool for the discrimination of materials of different chemical nature.

3.2. *Effect of the color of solids on acoustic waves*

After verifying that the first section of the acoustic wave (the first 100 μs) was not modulated by the dimensions of the solid, we decided to evaluate the influence of other physical properties; particularly, the scattering and the absorption of the incident photons reaching the target. To this end, plasmaphonies from the 6 colored epoxy resin cylinders and the non-pigmented reference were evaluated. Fig. 5 depicts the resulting acoustic signals. As shown, upon keeping all other parameters constant, the color of the analyzed solid altered the intensity of acoustic signal. This circumstance can be discussed on the basis of the different ε values (as well as transmission through and reflection from the solid surface) that the chromophore in each painting possesses. As a

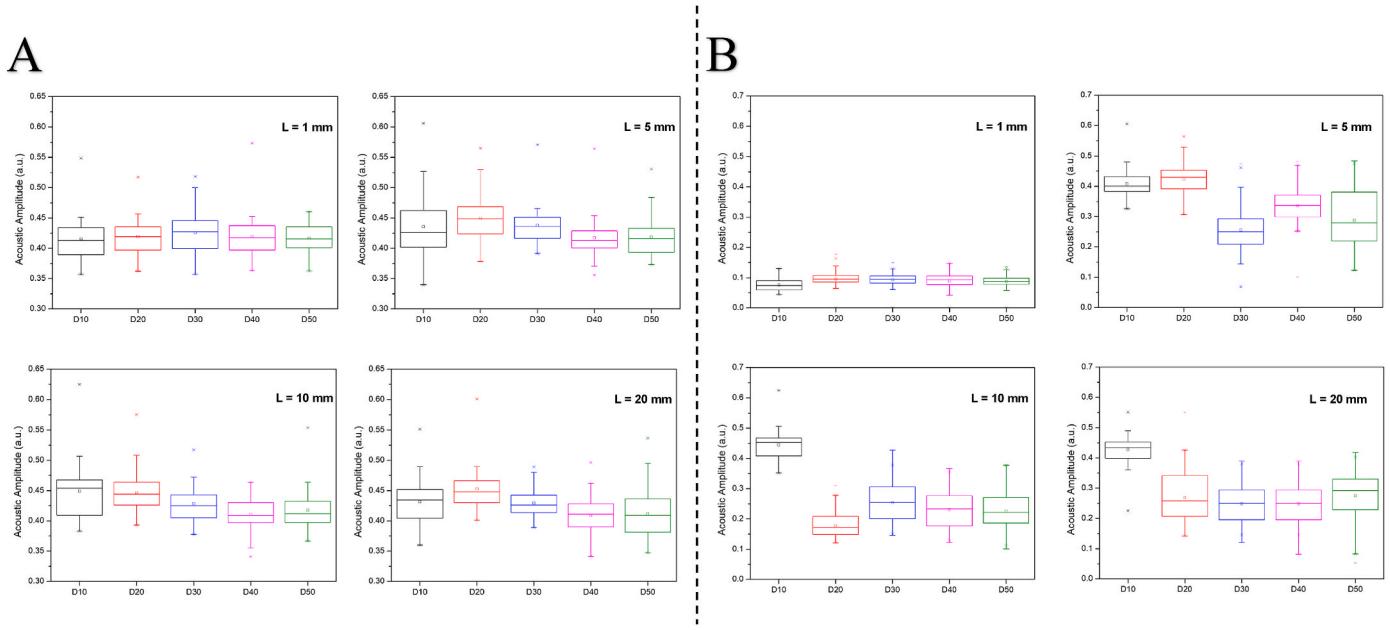

Fig. 4. Averaged max-to-min acoustic amplitude for 60 acoustic events produced by laser shots at the center of Al cylinders of different diameter (x axis) as a function of their length (1 mm, 5 mm, 10 mm and 20 mm) computed from A) the first max-to-min and B) the second max-to-min.

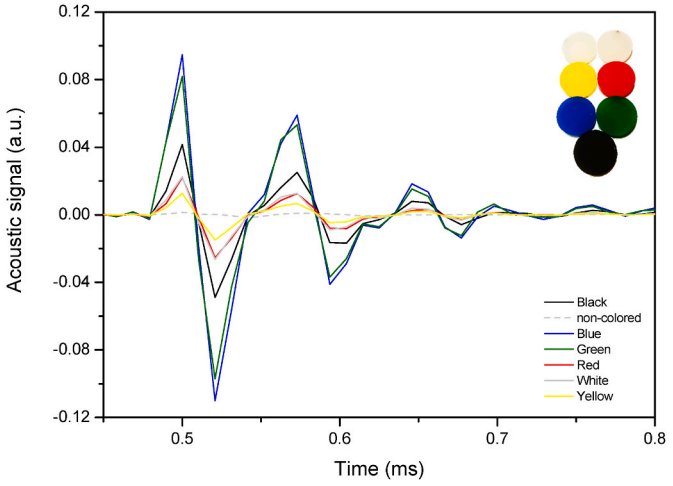

Fig. 5. Acoustic waves for plasmaphonies coming from colored epoxy cylinders.

rule of thumb, darker pigments in the VIS region are stronger near-infrared (NIR) absorbents than lightly-colored pigments. Data reported in Table 2S in the Supplementary Material summarize the averaged peak-to-peak acoustic amplitude (a.u.) scored for 25 successive plasmaphonies at 3 fresh sampling positions on the surface of the different colored epoxy cylinders together with their experimentally measured absorption % at 1064 nm using a continuous source of NIR light. As observed, in the case of the solids tested herein, most of the IR radiation was not absorbed, with the black cylinder being an exception. However, the maximum peak-to-peak acoustic amplitude was registered for plasmaphonies from the green and blue cylinders, thereby suggesting a better laser-matter coupling. Additionally, the departure from the expected trend could be indicative of photothermal effects on the solids. This hypothesis is backed by the fact that, in our configuration, successive laser shots impacted the same sampling spot. Absorption above a certain intensity threshold value of IR radiation is tied to temperature increases in the material. In this situation, the epoxy resin may become softened and changes in the absorbance spectra may occur [28]. As a consequence, alterations in the resulting plasmaphony intensity, such as those observed, may arise. While photothermal effects are expected to be emphasized for the dark-colored cylinders, they cannot be discarded for the rest of the solids. The results from this section clearly show that the absorption coefficient of a solid significantly influences the resulting plasmaphony. However, it is complex to extrapolate this influence to those solids for which absorption properties are likely to vary significantly along small regions.

3.3. *Effect of the inner porosity of solids on acoustic waves*

The hardness of the solid is another factor susceptible of influencing laser-matter coupling and, consequently, the acoustic signals. Hardness is roughly correlated to density. Closer packing of atoms results in greater density and shorter bond lengths, thereby giving greater hardness to the material. To this end, a total of 6 cylinders were *3D* printed. Two wires of different thickness, 0.178 mm (thin) and 0.254 mm (thick), were considered for each of the 3-samples batch. Porosity and bulk density within each batch of samples was varied by tuning the parameters of the printing process. Thus, cylinders with density of 0.50, 0.75 and 1.00 g·cm^{-3} for each type of wire were printed. Fig. 6 shows the representative sound waves for the tested samples printed from thin (Fig. 6A) and thick (Fig. 6B) wires, respectively.

As can be observed, no significant variations within the profile of the plasmaphonies from cylinders of distinct porosity were detected. However, a slight variation in the sound emission performance of *3D*-printed porous samples was identified. The thinner the wire, and subsequently, the lower the resulting porosity, the lower the acoustic signal was; at levels of 0.06 a.u. for the maximum amplitude value. The same hold true to the cylinder was printed using the thick wire at its highest-density (1.00 g cm-3). In contrast, as the density was reduced, thus the percentage of void space in the solid increased (when density of 0.75 g·cm^{-3} and 0.50 g·cm^{-3} for the thick wire) the acoustic amplitude increased a 30% up to 0.08 a.u. As expected, the porosity present in the solid can have a strong effect on some of their structural properties since the locally varying porosity modifies their elastic mechanical properties, i.e., the elastic modulus decreases with porosity.

While these results prove that the ratio of pore volume to the total volume of a solid affects the sensitivity of the ongoing plasmaphony, it is

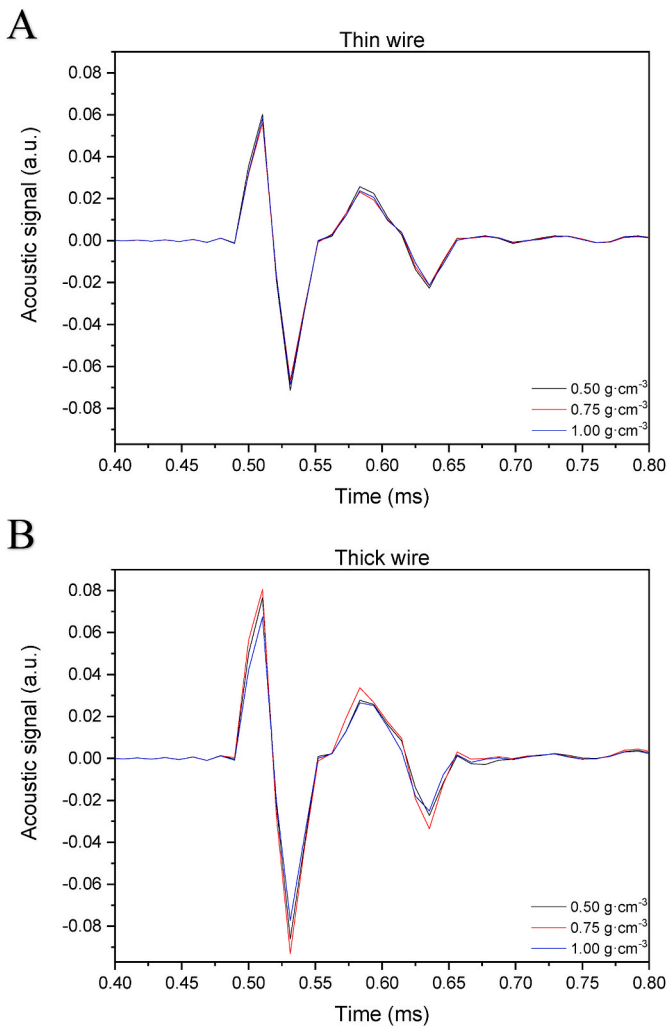

Fig. 6. Acoustic waves for plasmaphonies coming from 3D-printed cylinders from thin (A) and thick (6B) wires, respectively.

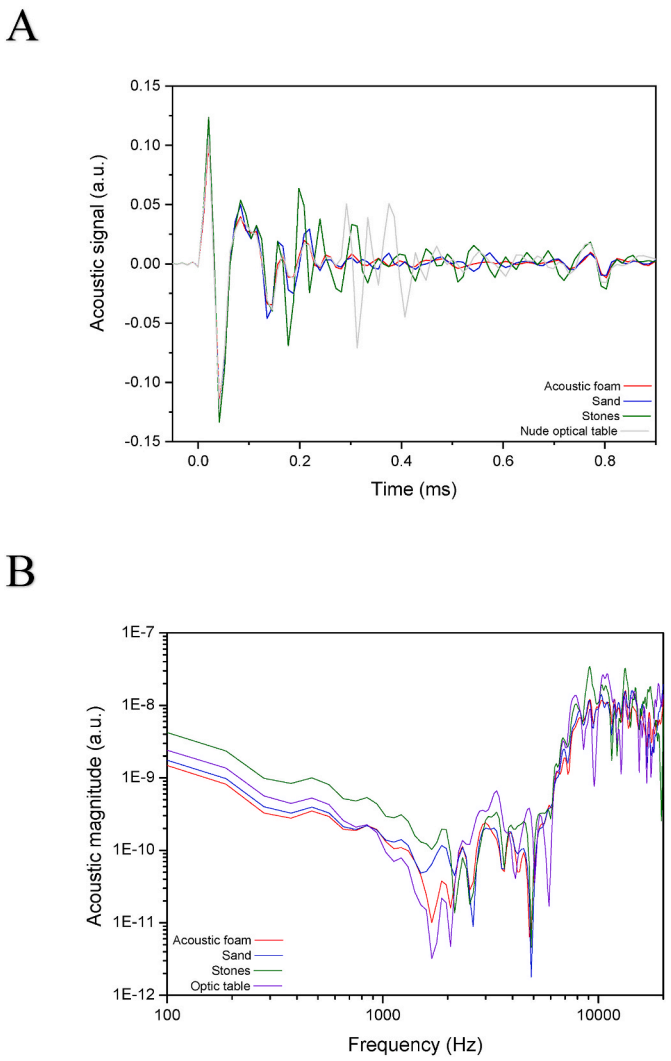

Fig. 7. A) Plasmaphonies waveforms of an Al cylinder (3 cm in diameter and 1 cm in length) when located over different surrounding terrains. B) FFT spectra of the waveforms.

also intricate to accurately move these results to natural materials, since the range of porosity for the polymeric cylinders evaluated herein may lay far away the intended range of applicability for some of them.

3.4. Effect of the surrounding terrain on acoustic waves

The influence on plasmaphonies from the same Al cylinder (30 mm in diameter and 10 mm in length) surrounded by three different ground surfaces covering the 50 cm distance between the target and the microphone (with the receiver being elevated at a height of 15 cm from the terrain) is illustrated in Fig. 7A. As can be observed, sound propagating over sandy terrain matched with that traversing over the polyurethane acoustic foam. Both surroundings tend to absorb undesired sound reflections and echoes and prevent them from distorting the acoustic waves. In contrast, the propagation of sound over a stone terrain showed components similar to those observed for the uncovered optical table, evidencing acoustic features attributable to echoes and resonances. As shown in Fig. 7B these artifacts caused by the ground reflective properties resulted in constructive and destructive interferences that altered the frequency profile of the sample acoustic spectrum. Terrain-induced differences as the sound wave propagates into the receptor can be outlined as characteristic dominant peaks emerged and disappeared. Moreover, the corresponding frequencies and relative amplitudes of these interferences depend on the location, size, depth and continuity of the scatterers. It is important to highlight that the first section of the acoustic signal in the time domain remained unaffected by the surroundings. This observation further linked that section of the wave to the laser-matter coupling process and also allowed us to consider its use for potential identifications of the solid being interrogated regardless of the environment in which it is located.

3.5. Effect of the coordinates of the microphone on acoustic waves

3.5.1. Microphone-to-sample distance

An acoustic source in a medium with no reflections experiences an intensity attenuation dependent on the distance traveled from the source towards the receiver, as given by the equation:

$$I = \frac{p^2(r)}{\rho c} = \frac{W}{4\pi r^2} \qquad \text{Equation 1}$$

where:

I = acoustic intensity (Watts·m^{-2})
$p(r)$ = sound pressure at radial distance r (N·m^{-2})
r = distance from the source in meters (m)
W = sound power (Watts)
$\rho\, c$ = acoustic impedance (rayls)

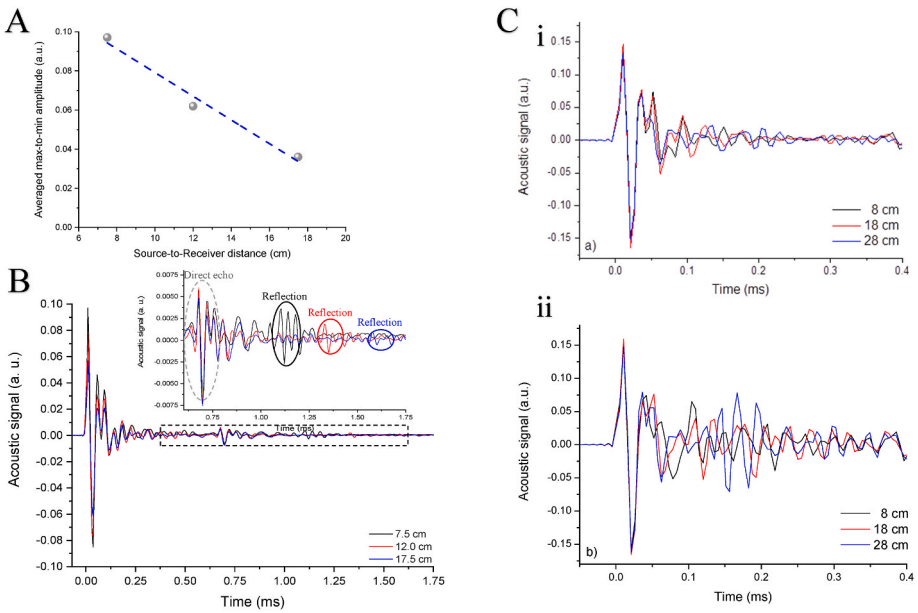

Fig. 8. *A) Averaged max-to-min acoustic amplitude attenuation according to source-to-receiver distance. B)* Waveforms for the plasmaphonies of an Al cylinder when located at increasing distances from the receiver over the same surrounding terrain. Inset shows in detail the direct echo and the ensuing reflections. C) Waveforms for the plasmaphonies of an Al cylinder when the receiver was located at variable heights from the ground over different surrounding terrains: C-i) sandy and C-ii) stony.

Fig. 8 reflects variations on sound waves from laser-produced plasmas as a function of mic coordinates to emitting source and floor. Fig. 8A plots the averaged acoustic amplitude of 20 plasmaphonies from an Al cylinder (30 mm in diameter, 10 mm in length) when located at 7.5, 12.0 and 17.5 cm, from the receiver, distances compatible with habitual LIBS setups. As shown, the data in Fig. 8A shows the *acoustic amplitude* as a linear function of r: AA = (0.140 ± 0.011)-(0.0061 ± 0.0009) × r, R = 0.9585. The averaged experimental acoustic amplitude fits a line due to the short range of distances covered, thus varying from the theoretical model of Equation (1). In addition to attenuation, the increases in distance may result in echo patterns caused by multiple reflections, thereby leading to a reflected wave propagating to the receiver along with the direct wave from the plasma source. Fig. 8B depicts acoustic signals in the time domain for plasmaphonies acquired under the three different source-to-receiver distances. The oscillations featured in early stages of the waves, while preserving a nearly identical profile, decreased with larger distances. Thus, from 0.125 ms onwards, the different waves traveling began to reveal differences among them and oscillation shifts could be observed. Furthermore, a distance-dependent replicate of the dominant peaks pattern was identified indicating a direct echo. After the direct echo (at $\underset{\sim}{}$ 0.68 ms), multiple reflections were collected at the receiver. From mathematical calculations over the transient sound, based on the round-trip path from the sample surface to the microphone membrane, theoretical reflections should occur at $\underset{\sim}{}$ 1.12 ms (for the shortest distance, 7.5 cm), 1.37 ms (for the middle distance, 12.0 cm) and 1.69 ms (for the largest distance, 17.5 cm). In good agreement with the calculated values, the corresponding experimental reflections were measured at 1.12 ms, 1.33 ms and 1.57 ms, respectively. These experimental delay values were directly proportional to the distance from the source and the receiver to the reflecting surface. In addition, as expected, the reflection intensity attenuated with increasing distance.

3.5.2. Microphone-to-ground height

The height of the receiver with respect to the ground is also a relevant variable to consider due to its potential influence on the acoustic wave. Fig. 8C compares the resulting plasmaphonies for different heights over diverse grounds (sandy (C-i) and stony(C-ii) terrains) at a source-to-receiver distance of 50 cm. Such a value was experimentally found to be the minimum distance necessary to record echo-free acoustic signals. Also note that the heights evaluated (8, 18 and 28 cm) were spatially limited by the dimensions of the anechoic chamber.

The different distances of the receiver to the ground generated different alterations in the sound propagation. Despite this, it should be stressed that the acoustic energy of the direct wave did not appear to be altered for the receiver heights considered in this experiment. As discussed in the previous section, we observed that the inference of those alterations was dependent on the type of terrain placed in the acoustic path (the so called "ground effect"). Thus, in the case of a stone ground, rocks reflected more acoustical energy resulting in a significantly different acoustic profile depending on the receiver-to-ground height. In contrast, sand particles yielded similar attenuation values no matter the height to the ground considered while the differences in acoustic propagation were much smaller.

All these observations suggest that the surface where the probed solid is located, together with the distance of the receiver as well as its height with respect to the ground may create a complicated acoustic structure upon arrival at the detector that further convolutes in time. Consequently, the acoustic ground- and coordinates-dependencies complicate assigning a specific plasmaphony to a solid interrogated by laser and should be carefully addressed.

3.6. Effect of the angle of incidence on acoustic waves

The angle existing between the acoustic emitting source and the receiver can also play an important role in the final recorded wave. As the collection angle varies so do incidence in the direct wave of reflections on the ground and echoes. For this experiment, plasmas were sparked on the surface of 6 identical Al plates (40 × 40 × 2 mm) at varying laser beam incidence angles. The angle for acoustic capturing was kept at $\theta_{cap} = 0^{\circ}$. Coordinates were set as follows: 48.5 cm microphone-to-target distance and 16.5 cm microphone-to-ground height. Acoustic foam was used as flooring to exclusively evaluate the influence of the angle of incidence. A goniometer was used to control the incidence angle of the laser beam on the target surface. The distance between the focusing lens and the target was conveniently adjusted for

each refreshed plate to preserve identical irradiance value at the target surface.

Fig. 9 displays the averaged sound waves for 180 plasmaphonies (a set of 30 laser events at 6 fresh positions each) induced at the center of the Al plates for incidence angles ranging from $\theta_i = 0^\circ$ (normal incidence) to $\theta_i = 50^\circ$ to the target. The asymmetry caused by oblique incidence of the laser beam implied a loss of symmetry of the acoustic source that led to an asymmetrical pattern of the acoustic waves. The comparison of multiple incidence configurations while keeping every other geometrical and physical parameters of the laser beam constant revealed negligible differences for the main amplitude, calculated as the difference between the absolute maximum and minimum of the waveforms. In contrast, more prominent differences could be identified at the tail of the waveform as the incidence angle increased. A plausible origin for such variations may be found in the restrictions imposed upon the expansion dynamics of the plasmas by the sample volume affected by the laser pulse and the subsequently produced ablation crater, which are bound to differ with θ_i. Alterations in the spatial profile of the plasma plume imply the formation of direction-dependent patterns for the laser-generated sound, that is, exclusive reflection coefficients each angle of the acoustic wavefront. The anisotropy of the acoustic wave is expected to increase as a function the optical and thermal characteristics of the solid material under inspection.

In summary, alterations of the solid surface affecting its acoustic reflection coefficients (e.g., irregular surface topography of the sample) result in severe variations for the propagation patterns of the laser-generated sound. A feasible use of the direction sensitivity could be deeper information on changes in the geometrical and physical-chemical properties of the inspected surface based on the laser-generated sound pattern. In this context, the correlation between the information recorded by multiple receivers located at different positions with respect to the sample could help reducing the possible negative impact of the direction dependency on the analytical signal while enhancing the sample-related data.

4. Conclusions

The implications on the collected laser-induced acoustic spectra of solids upon modification of internal parameters and sample surroundings are systematically addressed in the present work. First, effects caused by the dimensions of the solid, the sampling spot size, laser-matter coupling and internal porosity were evaluated. The resulting sound waves, which we have tagged here as plasmaphonies, were compared for a sets of Al cylinders featuring different diameters and lengths as well as equally-sized dyed epoxy cylinders and *3D*-printed solids of varying inner porosity. Results revealed a close relationship between the magnitude of the maximum-to-minimum acoustic amplitude and the physical-chemical properties of the solid. This magnitude was deduced to be intimately associated with the direct wave from the plasma source and is located within the first out of three well-defined sections identified during the lifetime of the acoustic signal. The aforementioned magnitude evidenced no influence of solids size and sampling position along its surface. In contrast, the dynamics of the solid surface after laser excitation seemed to strongly impact the later components of the sound waves where echoes and reflections of the sound wave have a relevant presence. In addition, acoustic signals from laser-induced plasmas showed a significant influence from the surrounding terrain where analysis of the solid is performed. While the first section of the time-domain acoustic signal remained unaltered, terrain conferred the acoustic wave a complex structure that became more raveled in time, concealing information pertaining to the sample. The same phenomenon was observed upon variation of the sample-to-receiver coordinates i.e., the microphone position above the ground and the angle at which it was positioned with respect to the surface of the solid, indicating large anisotropy in the signal. Although extracting information from acoustic signals to categorize a particular solid is challenging, the peculiarities of

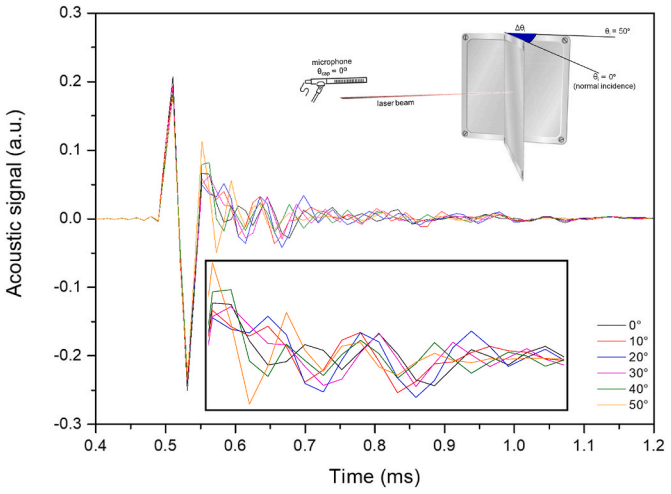

Fig. 9. Averaged (n = 180 plasmaphonies) sound waves induced at the center of the Al plates for incidence angles ranging from θi = 0° (normal incidence) to θi = 50° to the target. Inset zooms the time window between 0.55 ms and 0.75 ms to highlight differences induced by the change in sample-to-receiver angle.

the plasmaphonies make it possible to outline some relevant attributes of the solid, including its chemical nature, shape and size, and the acoustic behavior of the environment in which it is located. Therefore, upon thorough calibration of the parameters presented in this work, the detection of the acoustics generated by laser-induced plasmas in a solid may be employed as a complementary analytical tool toward a more complete identification of the samples interrogated.

Notes

The authors declare no competing financial interest.

CRediT authorship contribution statement

Markéta Bosáková: Formal analysis, Investigation, Data curation. **Pablo Purohit:** Formal analysis, Investigation, Data curation, Writing – original draft, Writing – review & editing. **César Alvarez-Llamas:** Conceptualization, Investigation, Software, Data curation, Writing – review & editing. **Javier Moros:** Conceptualization, Methodology, Formal analysis, Investigation, Validation, Writing – original draft, Writing – review & editing. **K. Novotný:** Validation, Writing – review & editing. **Javier Laserna:** Supervision, Writing – review & editing, Funding acquisition, Project administration.

Declaration of competing interest

The authors declare that they have no known competing financial interests or personal relationships that could have appeared to influence the work reported in this paper.

Data availability

Data will be made available on request.

Acknowledgments

The present research has been supported with funding provided by the projects UMA18-FEDERJA-272 from the Junta de Andalucía and PID2020-119185GB-I00 from Ministerio de Ciencia e Innovación, Spain. M.B. is grateful to the Specific Research Project, Masaryk University MUNI/A/1412/2021. P.P. is grateful to the European Union's Next Generation EU (NGEU) plan and the Spanish Ministerio de

Universidades for his Margarita Salas fellowship under the program "Ayudas para la Recualificación del Sistema Universitario Español".

Appendix A. Supplementary data

Supplementary data to this article can be found online at https://doi.org/10.1016/j.aca.2022.340224.

References

[1] A. Vogel, V. Venugopalan, Mechanisms of pulsed laser ablation of biological tissues, Chem. Rev. 103 (2003) 577–644.
[2] R.E. Russo, X. Mao, J.J. Gonzalez, V. Zorba, J. Yoo, Laser ablation in analytical chemistry, Anal. Chem. 85 (2013) 6162–6177.
[3] D. Pozebon, G.L. Scheffler, V.L. Dressler, Recent applications of laser ablation inductively coupled plasma mass spectrometry (LA-ICP-MS) for biological sample analysis: a follow-up review, J. Anal. At. Spectrom. 32 (2017) 890–919.
[4] E. Fadeeva, V. Khanh Truong, M. Stiesch, B.N. Chichkov, R.J. Crawford, J. Wang, E. P. Ivanova, Bacterial retention on superhydrophobic titanium surfaces fabricated by femtosecond laser ablation, Langmuir 27 (2011) 3012–3019.
[5] R. Suriano, A. Kuznetsov, S.M. Eaton, R. Kiyan, G. Cerullo, R. Osellame, B. N. Chichkov, M. Levi, S. Turri, Femtosecond laser ablation of polymeric substrates for the fabrication of microfluidic channels, Appl. Surf. Sci. 257 (2011) 6243–6250.
[6] H. Zeng, X.-W. Du, S.C. Singh, S.A. Kulinich, S. Yang, J. He, W. Cai, Nanomaterials via laser ablation/irradiation in liquid: a review, Adv. Funct. Mater. 22 (2012) 1333–1353.
[7] Y. Xu, L. Yan, X. Li, H. Xu, Fabrication of transition metal dichalcogenides quantum dots based on femtosecond laser ablation, Sci. Rep. 9 (2019) 2931.
[8] F.J. Fortes, J. Moros, P. Lucena, L.M. Cabalín, J.J. Laserna, Laser-induced breakdown spectroscopy, Anal. Chem. 85 (2013) 640–669.
[9] W.D. Hahn, N. Omenetto, Laser-induced breakdown spectroscopy (LIBS), Part I: review of basic diagnostics and plasma-particle interactions: still-challenging issues within the analytical plasma community, Appl. Spectrosc. 64 (2010) 335A–366A.
[10] Z. Wang, M.S. Afgan, W. Gu, Y. Song, Y. Wang, Z. Hou, W. Song, Z. Li, Recent advances in laser-induced breakdown spectroscopy quantification: from fundamental understanding to data processing, TrAC, Trends Anal. Chem. 143 (2021), 116385.
[11] F. Huang, M. Lei, J. Wang, D. Chen, T. Gao, X. Wang, Sound waves generated by nanosecond and femtosecond laser ablation on different metals, Optik 178 (2019) 1131–1136.
[12] G. Chen, E.S. Yeung, Acoustic signal as an internal standard for quantitation in laser-generated plumes, Anal. Chem. 60 (1988) 2258–2263.
[13] E. Schwarz, S. Gross, B. Fischer, I. Muri, J. Tauer, H. Kofler, E. Wintner, Laser-induced optical breakdown applied for laser spark ignition, Laser Part. Beams 28 (2010) 109–119.
[14] C. Stauter, P. Gérard, J. Fontaine, T. Engel, Laser ablation acoustical monitoring, Appl. Surf. Sci. 109–110 (1997) 174–178.
[15] S. Palanco, J. Laserna, Spectral analysis of the acoustic emission of laser-produced plasmas, Appl. Opt. 42 (2003) 6078–6084.
[16] A. Hrdlička, L. Zaorálková, M. Galiová, T. Čtvrtníčková, V. Kanický, V. Otruba, K. Novotný, P. Krásenský, J. Kaiser, R. Malina, K. Páleníková, Correlation of acoustic and optical emission signals produced at 1064 and 532 nm laser-induced breakdown spectroscopy (LIBS) of glazed wall tiles, Spectrochim. Acta B 64 (2009) 74–78.
[17] B. Chide, S. Maurice, N. Murdoch, J. Lasue, B. Bousquet, X. Jacob, A. Cousin, O. Forni, O. Gasnault, P.-Y. Meslin, J.-F. Fronton, M. Bassas-Portús, A. Cadu, A. Sournac, D. Mimoun, R.C. Wiens, Listening to laser sparks: a link between Laser-Induced Breakdown Spectroscopy, acoustic measurements and crater morphology, Spectrochim. Acta B. 153 (2019) 50–60.
[18] N. Murdoch, B. Chide, J. Lasue, A. Cadu, A. Sournac, M. Bassas-Portús, X. Jacob, J. Merrison, J.J. Iversen, C. Moretto, C. Velasco, L. Parès, A. Hynes, V. Godiver, R. D. Lorenze, P. Cais, P. Bernadi, S. Maurice, R.C. Wiens, D. Mimoun, Laser-induced breakdown spectroscopy acoustic testing of the Mars2020 microphone, Planet. Space Sci. 165 (2019) 260–271.
[19] P. Lu, Z. Zhuo, W. Zhang, J. Tang, T. Xing, Y. Wang, T. Sun, J. Lu, Determination of calorific value in coal by LIBS coupled with acoustic normalization, Appl. Phys. B 127 (2021) 82.
[20] S. Li, W. Weng, C. Kong, M. Aldén, Z. Li, Dual-laser-induced breakdown thermometry via sound speed measurement: a new procedure for improved spatiotemporal resolution, Sensors 20 (2020) 2803.
[21] G.J. Tserevelakis, P. Pouli, G. Zacharakis, Listening to laser light interactions with objects of art: a novel photoacoustic approach for diagnosis and monitoring of laser cleaning interventions, Herit. Sci. 8 (2020) 98.
[22] A. Papanikolaou, G.J. Tserevelakis, K. Melessanaki, C. Fotakis, G. Zacharakis, P. Pouli, Development of a hybrid photoacoustic and optical monitoring system for the study of laser ablation processes upon the removal of encrustation from stonework, Opto-electron. adv. 3 (2020), 190037-1–190037-11.
[23] S. Kradolfer, K. Heutschi, J. Koch, D. Günther, Listening with Curiosity – tracking the acoustic response of portable laser ablation, Chimia 75 (2021) 300–304.
[24] B. Chide, O. Beyssac, M. Gauthier, K. Benzerara, I. Estève, J.-C. Boulliard, S. Maurice, R.C. Wiens, Acoustic monitoring of laser-induced phase transitions in minerals: implication for Mars exploration with SuperCam, Sci. Rep. 11 (2021), 24019.
[25] M.R. Mofakhami, H.H. Toudeshky, S.H. Hashemi, Finite cylinder vibrations with different end boundary conditions, J. Sound Vib. 297 (2006) 293–314.
[26] F.J. Nieves, F. Gascon, A. Bayon, An analytical, numerical, and experimental study of the ax symmetric vibrations of a short cylinder, J. Sound Vib. 313 (2008) 617–630.
[27] F.O. Clark, R. Penney, W.E. Pereira, J. Kielkopf, J. Cline, A passive optical technique to measure physical properties of a vibrating surface, SPIE. Proc. Infrared. Remote Sens. Instrum. XXII. (2014), 92190G, https://doi.org/10.1117/12.2064366.
[28] E. Bormashenko, R. Pogreb, A. Sheshnev, E. Shulzinger, Y. Bormashenko, A. Katzir, IR laser radiation induced changes in the IR absorption spectra of thermoplastic and thermosetting polymers, J. Opt. Pure Appl. Opt. 3 (2001) 229–235.